Atmos. Meas. Tech. Discuss., 6, 9655–9688, 2013
www.atmos-meas-tech-discuss.net/6/9655/2013/
doi:10.5194/amtd-6-9655-2013


Atmospheric Measurement Techniques Discussions



# Peroxy radical detection for airborne atmospheric measurements using cavity enhanced absorption spectroscopy of $NO_2$

**M. Horstjann, M. D. Andrés Hernández, V. Nenakhov, A. Chrobry, and J. P. Burrows**

Institute of Environmental Physics, University of Bremen (IUP-UB), Otto-Hahn-Allee 1, 28359 Bremen, Germany

Received: 18 September 2013 – Accepted: 19 October 2013 – Published: 8 November 2013

Correspondence to: M. Horstjann (markus.horstjann@iup.physik.uni-bremen.de)

Published by Copernicus Publications on behalf of the European Geosciences Union.







## Abstract

Development of an airborne instrument for the determination of peroxy radicals (PeRCEAS – Peroxy Radical Cavity Enhanced Absorption Spectroscopy) is reported. Ambient peroxy radicals ($HO_2$ and $RO_2$, R being an organic chain) are converted to $NO_2$ by adding NO, and are recycled through subsequent reaction with CO and $O_2$, thus forming a chain reaction with an amplification factor called chain length. The concentration of $NO_2$ is measured by continuous-wave cavity ring-down spectroscopy (CRDS) using an extended cavity diode laser at 409 nm. Optical feedback from a V-shaped cavity optimizes resonator transmission and allows for a simple detector set-up. CRDS directly yields absorption coefficients, thus providing $NO_2$ concentrations without additional calibration. The optimum $1\sigma$ detection limit is 0.3 ppbv at an averaging time of 40 s and an inlet pressure of 300 mbar, corresponding to a concentration of $2 \times 10^9$ molecules $cm^{-3}$. The calibration of the PeRCEAS chain length at an inlet pressure of 300 mbar yields a value of $120 \pm 7$. The peroxy radical $1\sigma$ detection limit for an averaging time of 120 s and a chain length of 120 is $\sim$ 3 pptv.

## 1 Introduction

The hydroperoxy – ($HO_2$) and organic peroxy radicals ($RO_2$, R being an organic chain), hereafter referred to as peroxy radicals, are known for their importance in photochemical reaction cycles both in the stratosphere (e.g. Thrush et al., 1998) and troposphere (e.g. Monks, 2005). They are very reactive species, and in combination with the hydroxyl radical (OH) play a crucial role in most atmospheric oxidation mechanisms which lead to $O_3$, peroxy acetyl nitrate (PAN), aldehydes and acids. To fully characterize the photochemical status of the atmosphere, it is therefore highly desirable to include peroxy radical concentrations. Furthermore, for certain environments modelled and measured concentrations disagree to a significant amount, pointing towards a yet unknown radical recycling process (Lelieveld et al., 2008; Hofzumahaus et al., 2009; Whalley





AMTD
6, 9655–9688, 2013



et al., 2011). Although their ambient concentrations are generally low, peak mixing ratios of up to 100 pptv have been observed (Hofzumahaus et al., 2009).

A direct measurement of peroxy radicals remains a challenging task due to their high reactivity and thus short lifetime. The only existing technique for direct and speciated measurements is the Matrix Isolation Electron Spin Resonance Spectroscopy, which traps them in a $LN_2$-cooled $D_2O$ matrix. The required long sampling times of $\sim$ 30 min and the off-line analysis in the laboratory by probing their rotational transitions are important limitations of this technique (Mihelcic et al., 1985; Fuchs et al., 2009). Recent direct $HO_2$ detection set-ups by Djehiche et al. (2011), and Bell et al. (2012), employing cavity ring-down spectroscopy and noise-immune cavity enhanced heterodyne detection, respectively, still lack the necessary sensitivity for ambient measurements.

A well-known technique to indirectly measure the sum of peroxy radicals [$RO_2^*$] (:= [$HO_2$] + $\sum$[$RO_2$]) is the Peroxy Radical Chemical Amplification (PeRCA – complete nomenclature in Table 1),which facilitates a chain reaction of peroxy radicals into less reactive species (e.g. $NO_2$), whose concentration is then measured (Cantrell and Stedman, 1982; Cantrell et al., 1984; Hastie et al., 1991). The chain reaction increases the sensitivity to peroxy radicals as the number of $NO_2$ molecules to measure is multiplied by the chain length. This parameter has to be calibrated in order to determine the peroxy radical concentration. For Chemical Mass Ionization Spectroscopy (CIMS), the radicals are converted to $H_2SO_4$, whereas for Laser-induced Fluorescence (LIF) OH is the end product being measured. These and other techniques are described in more detail in e.g. Heard (2006). The PeRCA variant which produces $NO_2$ is complemented by e.g. Chemiluminescence Detection, Laser-Induced Fluorescence or Tunable Diode Laser Spectroscopy (Heard, 2006) to measure its concentration. A highly sensitive chemical method using chemiluminescence detection is the reaction of $NO_2$ with a luminol (3-aminophthalhydrazide: $C_8H_7N_3O_2$) solution. Together with the PeRCA technique, this method yields excellent ($3\sigma$) detection limits for the total sum of peroxy radicals of 3 pptv (chain length $\sim$ 45, pressure 200 mbar, averaging time 20 s) and it has been used in numerous measurement campaigns, both ground-based (Burkert





AMTD
6, 9655–9688, 2013



et al., 2001a, b, 2003; Andrés Hernández et al., 2001; Andrés-Hernández et al., 2013) and airborne (Andrés Hernández et al., 2009, 2010; Kartal et al., 2010). Although well established for airborne measurements, the luminol detector still presents some drawbacks like its range of linearity and the dependency of the sensitivity to humidity and pressure (Wendisch and Brenguier, 2013). In order to overcome these limitations the PeRCEAS instrument was developed at the Institute of Environmental Physics, and it employs a variant of laser absorption spectroscopy called Cavity Ring-Down Spectroscopy (CRDS) to measure the $NO_2$ concentration. A V-shaped optical resonator provides optical feedback to the employed extended cavity diode laser (ECDL), stabilizing the laser emission wavelength and enhancing the cavity throughput.

A similar configuration using the PeRCA technique and a CRDS $NO_2$ detector (albeit without optical feedback) is described in Liu et al. (2009), who reported on an instrument for field measurements at standard pressures. It is a combination of a $NO_2$ CRDS detector (Hargrove et al., 2006) and a 5 m long (Teflon) tubing system enabling the peroxy radical chemical conversion. Its chain length is calibrated using rather high amounts of $HO_2$ between 0.5 and 3 ppbv generated by thermal decomposition of $H_2O_2$ (the PeRCEAS chain length calibration is described in Sect. 3.2). Investigation of the dependency of the chain length on ambient air humidity is not mentioned. The $NO_2$ detector is employing a Nd-YAG pumped dye laser and a resonator incorporating mirrors with a distance of 1 m (the PeRCEAS $NO_2$ detector is described in Sect. 2.2).

The chemical conversion of peroxy radicals to $NO_2$ in a chain reaction is facilitated by adding NO and CO to the sample air, thus enabling the reactions

$$HO_2 + NO \rightarrow OH + NO_2 \quad \text{(R1)}$$

and

$$OH + CO + O_2 + M \rightarrow HO_2 + CO_2 + M. \quad \text{(R2)}$$

The $HO_2$ radical is recycled, thus forming a chain reaction producing $NO_2$ which is subsequently measured.





AMTD
6, 9655–9688, 2013



The $RO_2$ radicals are contributing to the $NO_2$ concentration by

$$RO_2 + NO \rightarrow RO + NO_2, \quad \text{(R3)}$$

before also taking part in the chain reaction via $HO_2$

$$RO + O_2 \rightarrow HO_2 + \text{aldehydes}. \quad \text{(R4)}$$

Thus, both $HO_2$ and $RO_2$ convert NO to $NO_2$ via the chain reaction involving $HO_2$.

Additionally, also OH and RO radicals contribute to the $NO_2$ concentration via the mechanisms described above, but can be neglected due to their comparably low abundance in the atmosphere. The background concentration $[NO_2]_{ambient}$ is enhanced both by species reacting with NO (e.g. ozone) or by being (thermally) decomposed in the inlet (e.g. peroxyacetyl nitrate).

The resulting $[NO_2]_{meas}$ concentration measured is thus composed of

$$[NO_2]_{meas} = [NO_2]_{ambient} + [NO_2]_{other} + CL \times [RO_2^*], \quad (1)$$

where

$$[RO_2^*] := [HO_2] + \sum [RO_2], \quad (2)$$

neglecting both OH and RO. The PeRCA technique usually operates alternatingly between a so called "amplification mode" (CO is added, so the chain reaction takes place) and a "background mode" (where CO is replaced with $N_2$, suppressing the chain reaction). The background mode thus only measures the first two addends of (1), and the difference in the $NO_2$ concentration between amplification and background mode constitutes the peroxy radical mediated part. Thus

$$\Delta[NO_2] := [NO_2]_{ampl} - [NO_2]_{backgr} = CL \times [RO_2^*]. \quad (3)$$

The chain length CL can be determined by sampling known peroxy radical mixtures under controlled conditions, and can then be used to determine the peroxy radical concentrations of the sampled air.





AMTD
6, 9655–9688, 2013



The $NO_2$ concentration is measured by cavity ring-down spectroscopy (CRDS), a technique well known for its sensitivity and robustness. Already employed in 1988 for absorption measurements (O'Keefe and Deacon, 1988), it is nowadays one of the dominant trace gas absorption measurement techniques. Reviews of this spectroscopy method may be found in (Busch and Busch, 1999) or, more recently, in (Berden and Engeln, 2010). Briefly, a resonator consisting of highly reflective mirrors is filled with the sample air to be measured. Usually a laser is used for resonator excitation, and if a certain resonator transmission intensity is reached, the laser is switched off rapidly. The subsequent decay of this transmission yields the ring-down time $\tau$ after which the intensity has decayed to $e^{-1}$ of its initial value. The losses leading to this decay incorporate absorption and scattering both from the mirrors themselves and from the sample air. The absorption coefficient $\alpha$ of an absorber of interest can be calculated directly from two ring-down time measurements; one with the sample air inside the resonator not containing the absorber (yielding $\tau_0$) and one with the absorber present (yielding $\tau_\alpha$):

$$\alpha = \frac{n}{c_0} \times \left( \frac{1}{\tau_a} - \frac{1}{\tau_0} \right), \tag{4}$$

where $n$ is the index of refraction (here: of the sample air), and $c_0$ is the speed of light in vacuum.

The $NO_2$ concentration $\frac{N}{V}$ can then be calculated using

$$\alpha = \frac{N}{V} \times \sigma_{NO_2}^{409\,nm} \tag{5}$$

where $N$ is the number of molecules, $V$ is the volume, and $\sigma_{NO_2}^{409\,nm} \sim 6.5 \times 10^{-19}\,cm^2\,molecule^{-1}$ is the absorption cross section at a wavelength of 409 nm, a temperature of 296 K and a pressure of 300 mbar (Vandaele et al., 2002; Nizkorodov et al., 2004).





AMTD
6, 9655–9688, 2013



## 2 Experimental

Figure 1 shows the schematic set-up of the PeRCEAS instrument developed for operation on the research aircraft HALO (High Altitude and LOng Range Research Aircraft – see http://www.halo.dlr.de/ for further information). The PeRCEAS instrument can be divided in two main parts; the inlet (outer dimension 73 cm × 32 cm × 24 cm; total weight 21 kg), which is installed in the aircraft fuselage to sample the outside air, and the $NO_2$ detectors analysing the sampled (and chemically converted) air. The sampled air proceeds either through a bypass, which is used for the inlet pressure regulation, or to the reactors and $NO_2$ detectors to be measured. The latter is then scrubbed of $NO_x$ and CO before being merged with the bypass flow again. The $NO_2$ detectors are mounted in a customized HALO 19″ rack (outer dimension 170 cm × 65 cm × 55 cm; mounted total weight 140 kg), which also contains the HALO power supply distribution, a 15″ monitor (VISAM GmbH), a local power distribution unit (Stachl Elektronik GmbH), the laser power supply, a DAQ (data acquisition) PXI computer (National Instruments), two Peltier temperature controllers (type MPT 10000, Wavelength Electronics) and one pressure and 9 mass flow controllers (Bronkhorst Mättig GmbH). The rack bottom also contains a drawer which houses a 600 ppmv NO in $N_2$ – and a 10 ppmv $NO_2$ in synthetic air gas cylinder (for calibration purposes) and the corresponding pressure reducers. Figure 2 shows the assembled PeRCEAS rack.

Additionally required components are a pure CO and a $N_2$ gas cylinder, a $NO_x$ and a CO scrubber, and a vacuum pump (Scrollvac SC 30 D, Oerlikon Leybold Vakuum). For safety reasons, the CO gas cylinder is placed in a specially designed containment. The whole system including the inlet has a weight of 250 kg.

### 2.1 Inlet

Figure 3 shows the inlet gas handling and Fig. 4 a photograph of the PeRCEAS inlet. It was developed based on previous experience with a DUALER inlet (Kartal et al., 2010; Chrobry, 2013). The inlet is made of Teflon-coated stainless steel and consists





AMTD
6, 9655–9688, 2013



of a pressure controlled chamber (volume $\sim 100\,cm^3$), into which the sample air is sucked through a cone with a 1.2 mm orifice at its top, and cylindrical reactors (inner diameter 17 mm, length 500 mm, volume $\sim 110\,cm^3$) where the amplified conversion of peroxy radicals to $NO_2$ takes place. They are directly connected to the CRDS $NO_2$ detectors via $1/4''$ outer diameter black PFA tubing.

The chamber pressure is stabilized using a pressure sensor (type DMP 331, BD Sensors GmbH)/pressure regulator (Bronkhorst Mättig GmbH) combo. A reactor flow of 1 sLpm (standard Litres per minute) is achieved for inlet pressures from 200 to 900 mbar. A retention time of $\geq 1$ s is necessary for the complete peroxy radical conversion, which for the PeRCEAS reactors is exceeded for pressures $> 100$ mbar. An inlet pressure of 300 mbar decreases the relative humidity of the sample air to $\sim 10\,\%$, minimizing the deterioration of the chain length at high ambient relative humidity levels (Reichert et al., 2003).

In the amplification mode a mixture of 0.09 sLpm pure CO and 0.01 sLpm 600 ppmv NO in $N_2$ is added at the reactor top (addition point 1, Fig. 4), whereas 0.09 sLpm $N_2$ is added at the reactor bottom (addition point 2). In the background mode, the CO and $N_2$ addition is exchanged ($N_2$ and NO addition at reactor top, CO at reactor bottom). The CO mixing ratio of 9 %vol ensures a high chain length but is still well below the 12 %vol mixing ratio that poses the danger of creating explosive mixtures. The rerouting of the added gases between the addition points is facilitated by Teflon three-way magnetic valves (type QE 622, Staiger GmbH). The NO gas is scrubbed by $FeSO_4$, removing non-negligible traces of $NO_2$, before being added to the gas stream of the reactor top.

The measurement flow and its composition thus always remains the same (81 %vol sample air, 9 %vol CO, $\sim 10$ %vol $N_2$, and 6 ppmv NO). Of course, the composition of the sample air changes, at the least due to the additional amount of $NO_2$ stemming from the peroxy radical conversion.

To ensure a thorough mixing of the sample air with the added gases, the latter are distributed by eight circularly arranged ⌀ 1.5 mm orifices into the reactor. The cylindrical reactors end at the top in a truncated cone (4 mm top diameter, 14.2 mm height)





AMTD
6, 9655–9688, 2013



protruding into the pressure chamber. The shape and dimensions of these reactor inlets have been selected to prevent diffusion of the added gases into the pressure chamber while minimising the radical wall losses.

The inlet was thoroughly characterized regarding its operating conditions utilizing a luminol chemiluminescence $NO_2$ detector (Chrobry, 2013). For one reactor the chain length is $100 \pm 13$ at an inlet pressure of 300 mbar for a Teflon-coated cone orifice of 1.2 mm, and decreases to $\sim 84 \pm 8$ for an orifice of 1.0 mm. It drops to $55 \pm 8$ if an uncoated cone is used, emphasizing the importance of the choice of material to avoid radical wall losses. For the other reactor these values are $79 \pm 9$, $65 \pm 6$ and $44 \pm 6$, respectively, so the chain lengths of both detectors agree within their experimental errors.

The size of the inlet sampling orifice determines the operating pressures and flows of the instrument. For measurements at low ambient pressure (i.e. high altitude), the biggest orifice of 1.5 mm which minimizes the pressure difference between the inlet chamber and the ambient air ($\sim$ 40 mbar) should be chosen.

### 2.2 $NO_2$ detector

The $NO_2$ detectors in their current stage stem from research on optical feedback cavity-enhanced absorption spectroscopy (OF-CEAS), as reported in Morville et al. (2005), and Courtillot et al. (2006). Briefly, a V-shaped resonator consisting of three highly reflective mirrors is excited via a wavelength-scanning continuous-wave laser. Optical feedback from the resonator forces the laser to stabilize itself onto the resonator resonance, yielding broad transmission lines. Resonator optical losses can be calculated from these transmissions if their maxima are calibrated with a ring-down time measurement. OF-CEAS thus outputs absorption spectra with a wavelength resolution governed by the resonator's free spectral range. For an optimum configuration the distance between laser and resonator must be stabilized (usually by a mirror mounted on a piezo stack) using the symmetry of the transmission lines as an error signal.





AMTD
6, 9655–9688, 2013



The effect of optical feedback was characterized (Horstjann et al., 2012), and cavity transmissions with and without it during a laser scan can be seen in Fig. 5. The laser linewidth decreases about three orders of magnitude, and is temporarily locked to the resonator, yielding high resonator transmission (up to 1 % of the input power) which can be captured by a common Si photodiode detector.

The $NO_2$ detection limit for the detector using the OF-CEAS technique was determined to be $\sim 4$ ppbv for 1 s averages and a resonator pressure of 290 mbar. For the detection of $NO_2$ in an aircraft environment, the OF-CEAS detection scheme proved to be too susceptible to both temperature variation and vibration, therefore the more robust technique of cavity ring-down spectroscopy (CRDS) was implemented, albeit still with optical feedback and thus high resonator transmission.

The set-up of the detector is schematised in Fig. 6, and Fig. 7 shows a photo of the 19″ case containing the ECD Laser (type DL-100L, wavelength 409 nm, 13 mW output power, 20 GHz modehop free tuning range, Toptica Photonics AG), the Si photodiode detector (type HCA-S, bandwidth 2 MHz, gain $5 \times 10^5$ $VA^{-1}$, Femto Messtechnik GmbH), a DAQ connection board, a power supply distribution board, a piezo stabilizing circuit (Floralis, France) and a fast TTL switch-off signal generator (Stachl Elektronik GmbH), cables, and gas flow components. The optical detector consists of an aluminium cuboid with a recess. All optical components are fixed onto this cuboid, i.e. a $\lambda/2$ plate/polarization beam splitter combo (to adjust the optical feedback level), a prism on a manual linear stage (coarse adjustment of the laser-resonator distance), a mirror mounted onto a piezo stack (type P885.10, PI Ceramic GmbH) for fine adjustment of the laser-resonator distance, and the photodiode detector. The cuboid is mechanically isolated from the 19″ chassis by steel springs, and temperature isolated through 2 mm thick aluminium sheets covered with Armaflex AF isolation material (Armacell Enterprise GmbH). Its temperature is also actively stabilized by a Peltier element (type CP-031, Te Technology Inc.). The sample air flow enters in the cuboid center and exits on both ends through NPT-threaded connections, and its temperature, pressure and relative humidity are measured. No aerosol or other gas filtering is used, and no





AMTD
6, 9655–9688, 2013



adverse effects from mirror exposition to ambient air was experienced. At an inlet pressure of 300 mbar, the residence time of the sample air inside the resonator is ~ 5 s.

The V-resonator is formed by a recess in the cuboid (volume ~ 300 $cm^3$), sealed on top by a glued-in lid and on its sides by the glued-in highly reflective mirrors (diameter 1/2″, roc 100 cm, AT Films). The lid itself contains small plates sealed with o-rings, which can be opened to clean the mirrors. The mirror-to-mirror distance is 40 cm, and the measured vacuum peak ring-down times of ~ 26 µs yield an average mirror reflectivity of 99.995 % and a maximum light path of ~ 8 km. For a resonator pressure of 285 mbar, the ring-down time is ~ 20 µs and the light path thus ~ 6 km. The ring-down times garnered in the amplification and background modes directly yield the absorption coefficient of the $NO_2$ that was formed by the peroxy radical chemical conversion. Changing background concentrations of substances contributing to the $NO_2$ background are thus automatically accounted for if the change is slow compared to the duration of one background and one amplification mode measurement (~ 120 s).

The detector exhaust flows are purified by an activated charcoal scrubber removing the $NO_x$ traces and a Pt/Al pellets scrubber converting CO to $CO_2$ at temperatures $T > 195$ °C before being merged with the inlet bypass flow (Fig. 1).The laser is scanned over 10 GHz at a wavelength of 409 nm, and if a certain resonator transmission threshold is reached, a fast (< 1 µs) TTL signal is generated and fed to a FET circuit in parallel to the laser diode which then draws the current, effectively switching off the laser. The ring-down signal is then sampled with (1 MSample) $s^{-1}$ by a PXI-DAQ card (type PXI-6132, National Instruments), saved and analyzed with a PXI-computer (PXI-8105) by a custom LabVIEW program performing non-linear least-squares fits (Levenberg-Marquardt algorithm). The software provides 1 s-averaged ring-down values for online monitoring. Pressure-, flow-, temperature- and humidity sensor data is sampled at (1 Sample) $s^{-1}$ (PXI-6129) and shown also by the LabVIEW program.





AMTD
6, 9655–9688, 2013



## 3 Results and discussion

Accurate calculation of peroxy radical mixing ratios demands the knowledge of both the chain length (CL) and the $NO_2$ mixing ratio. The latter is straightforward as the CRDS technique yields absorption coefficients that translate into concentrations if the absorption cross section $\sigma_{NO_2}$ is known. Mixing ratios can then be calculated with the temperature and pressure of the sample air. The detector sensitivity was determined by a ring-down time background measurement of synthetic air. The chain length of the PeRCEAS instrument was experimentally determined for an inlet pressure of 300 mbar by generating a set of known $HO_2$ mixing ratios. The chain length is then determined by $CL = \Delta x_{NO_2} / x_{HO_2}$. The peroxy radical detection limit is calculated by dividing the $NO_2$ detection limit by the chain length.

### 3.1 $NO_2$ detection limit

To assess the detection limit of the $NO_2$ optical detector synthetic air was provided to the inlet cone, and a flow of 1 sLpm was drawn by the detector. The inlet chamber pressure was kept constant at 300 mbar. The measurement lasted 35 min, and Fig. 8 shows 1 s averages of the ring-down times recorded. The $1\sigma$ standard deviation is 0.08 µs, corresponding to a detection limit of the absorption coefficient of $6.7 \times 10^{-9}$ cm$^{-1}$ $(\sqrt{\text{Hz}})^{-1}$ or a mixing ratio of 1.5 ppbv $(\sqrt{\text{Hz}})^{-1}$ at an inlet pressure of $p = 300$ mbar and a temperature $T = 296$ K. Figure 9 shows the corresponding Allan variance (Allan, 1966), indicating an optimum averaging time of ~ 40 s with a minimum detectable mixing ratio of 0.3 ppbv. Longer averaging times are influenced by slow temperature drifts affecting both the laser and the resonator characteristics. For peroxy radical measurements the duration of a background and amplification mode is set to 60 s to allow for the gas flow to settle (see Fig. 12). The $NO_2$ detector sensitivity was tested for different concentrations of $H_2O$, CO and NO, and no significant variation was observed.





AMTD
6, 9655–9688, 2013



### 3.2 Chain length calibration

The chain length of the PeRCEAS instrument was calibrated using a $HO_2$ source introduced by Schultz et al. (1995); the employed model resembling the one characterized by Stöbener (1999), and described in detail by Reichert et al. (2003). Briefly, synthetic air is enriched with a known amount of water, flown through a quartz glass tube and provided to the PeRCEAS inlet. Shortly before being sucked in, the air is illuminated by a Hg/Ne gas UV lamp (type Pen-Ray, LOT-QuantumDesign GmbH), thus water is photolysed and $HO_2$ is produced. A photomultiplier tube (PMT, type 1259 with a $MgF_2$ window, Hamamatsu Photonics) measures a portion of the transmitted intensity afterwards. For the configuration employed, the $HO_2$ concentration can be calculated using

$$[HO_2] = \frac{\sigma_{H_2O}^{184.9\,nm}}{\sigma_{O_2}^{184.9\,nm}} \times \frac{[H_2O]}{[O_2]} \times [O_3], \quad (6)$$

where $\sigma_{H_2O}^{184.9\,nm} = (7.14 \pm 0.2) \times 10^{-20}\,cm^2\,molecule^{-1}$ is the absorption cross section of $H_2O$ at 184.9 nm (Cantrell et al., 1997; Hofzumahaus et al., 1997) and $\sigma_{O_2}^{184.9\,nm} = (1.6 \pm 0.08) \times 10^{-20}\,cm^2\,molecule^{-1}$ is the absorption cross section of $O_2$ (Hofzumahaus et al., 1997). $[H_2O]$ is calculated from measurements of a dew point sensor (type DMP 248, Vaisala GmbH). $[O_2]$ is given by the specifications of the used synthetic air gas cylinder (type Alphagaz, Air Liquide Deutschland GmbH).

To generate a range of different $HO_2$ concentrations, pure $N_2O$ gas is used as an optical filter (Cantrell et al., 1997) and absorbs part of the UV light prior to the quartz glass tube where the photolysis takes place. Since a measurement of small ozone concentrations is highly inaccurate, the measured PMT signal $I$ is instead used as an $[O_3]$ proxy (Kartal, 2009):

$$\frac{[O_3]}{[O_3^{max}]} = \frac{I}{I_{max}}. \quad (7)$$





AMTD
6, 9655–9688, 2013



The maximum ozone concentration ($[O_3^{max}]$) generated by the radical source was measured in the PeRCEAS $NO_2$ detector while adding 0.01 sLpm of 600 ppmv NO in $N_2$ to the reactor to convert the ozone to $NO_2$. The UV light was modulated by means of a mechanical shutter every seven minutes for a five minute background measurement. Figure 10 shows a measurement at an inlet pressure of 300 mbar which lasted 45 min. The ring-down time differences yield $x(O_3^{max}) = (4.0 \pm 0.6)$ ppbv, which together with the PMT measurement $I_{max} = 3.54$ V results in $x(O_3^{max})/I_{max} \sim (1.13 \pm 0.17)$ ppbv $V^{-1}$. This ratio compares reasonably well to a value of 0.96 ppbv $V^{-1}$ determined with a luminol chemiluminescence detector.

For the radical source used in this experiment the mixing ratios are $x(O_3^{max}) \sim 4$ ppbv, $x(H_2O) \sim 2000$ ppmv, and $x(O_2) \sim 20$ %vol, thus $x(HO_2^{max}) \sim 200$ pptv.

The uncertainty of the $HO_2$ concentration amounts to ±16 %, and consists of the uncertainties for the absorption cross sections of $H_2O$ (3 %) and $O_2$ (5 %), for the $H_2O$ concentration (2.5 %, from the dew point sensor variation), and for the $O_3$ concentration (15 %). The $O_2$ concentration uncertainty is negligible.

Multiple $HO_2$ calibrations have been carried out for both PeRCEAS reactors. For this, the radical source stepwise produced $HO_2$ mixing ratios of (10–200) pptv for ten minutes each, while the PeRCEAS reactors alternate between background and amplification mode every two minutes. An example of such a measurement at an inlet pressure of 300 mbar can be seen in Fig. 11, and Fig. 12 shows a transition process in detail. The switching of the magnet valves induces a pressure pulse, and it takes about 16 s for the gas flow to stabilize itself afterwards. A part of this settling time is caused by the residence time of the sample air inside the reactor (3 s), the tube connecting the inlet and $NO_2$ detector (< 1 s) and the detector itself (5 s).

The resulting chain length determination is shown in Fig. 13. The $NO_2$ errors were calculated from averaging the background respectively amplification ring-down times for a constant $HO_2$ mixing ratio. The chain lengths for the two reactors present in PeRCEAS are $CL_1 = 120 \pm 7$ and $CL_2 = 104 \pm 12$. The values agree within their





AMTD
6, 9655–9688, 2013



experimental error, but different chain lengths can also be attributed to small differences in the fabrication of the reactors.

These values are significantly higher than those determined with the luminol $NO_2$ detectors (Chrobry, 2013) of $100 \pm 13$ and $79 \pm 9$. This can be partly explained by different NO mixing ratios used (6 ppmv for PeRCEAS, 3 ppmv for the luminol detector). In order to find out other possible reasons for the difference a systematical sensitivity study was conducted, during which a series of measurements was taken with different synthetic air flows through radical source. It was found that for the inlet cone 1.2 mm diameter orifice and the flow quantity used in Chrobry (2013), outside air is sucked in even if the orifice is immersed in the quartz glass tube providing the air flow.

For an inlet pressure of 200 mbar PeRCEAS chain lengths of $74 \pm 12$ were determined, indicating higher radical inlet losses prior to the chemical conversion and amplification, which are most probably due to more turbulent flow conditions and increased radical-wall loss reactions.

## 4 Summary and conclusion

The development and characterisation of a peroxy radical chemical amplification instrument with a CRDS $NO_2$ detector for airborne measurements is reported. The $\Delta NO_2$ detection by CRDS allows for the direct calculation of the $RO_2^*$ mixing ratios without requiring a $NO_2$ calibration, and its sensitivity is free from interference of variations in the humidity and pressure levels. An optimum averaging time of 40 s yields a ($1\sigma$) minimum detectable $NO_2$ mixing ratio of 0.3 ppbv (resonator pressure 285 mbar).

For an inlet pressure of 300 mbar, the chain lengths of the reactors are $CL_1 = 120 \pm 7$ and $CL_2 = 104 \pm 12$, and the ($1\sigma$) detection limit of $RO_2^*$ ($:= [HO_2] + \sum[RO_2]$) is $\sim 3$ pptv for an averaging time of 120 s (duration of one background and one amplification mode measurement). For an inlet pressure of 200 mbar chain lengths of $74 \pm 12$ and a ($1\sigma$) detection limit of $\sim 4$ pptv (averaging time of 120 s) was determined.





AMTD
6, 9655–9688, 2013



The PeRCA-CRDS instrument reported by Liu et al. (2009) differs both in scope (airborne measurements for PeRCEAS vs. field measurements) and general layout (pressure stabilized inlet of PeRCEAS vs. Teflon tubing inlet, compact 19″ $NO_2$ detector with a diode laser for PeRCEAS vs. more voluminous Nd-YAG pumped dye laser set-up). Its chain length is reported to be $150 \pm 50$ for standard pressure. Both instruments show peroxy radical ($1\sigma$) detection limits of $\sim$ 3 pptv, albeit at different averaging times (120 s for PeRCEAS instead of 60 s), and at different inlet pressures (300 mbar for PeRCEAS instead of $\sim$ 1000 mbar).

As shown the PeRCEAS airborne instrument provides a means to measure peroxy radicals with suitable sensitivity and accuracy for the concentrations expected in the upper layers of the troposphere. It is currently certified for aircraft operation, and will take part in the OMO mission onboard the HALO aircraft, whose start is currently scheduled for end-2014.

*Acknowledgements.* We are indebted to the university mechanical workshop, especially for crafting the V-resonators. We acknowledge funding for this study by the University of Bremen, the State of Bremen, and the HALO SPP 1294 (Atmospheric and Earth system research) grant from the DFG Deutsche Forschungsgemeinschaft including salary funding for the first author.

## References

Allan, D. W.: Statistics of atomic frequency standards, Proc. IEEE, 54, 221–230, 1966. 9666

Andrés Hernández, M. D., Burkert, J., Reichert, L., Stöbener, D., Meyer-Arnek, J., and Burrows, J. P.: Marine boundary layer peroxy radical chemistry during the AEROSOLS99 campaign: measurements and analysis, J. Geophys. Res., 106, 20833–20846, 2001. 9658

Andrés-Hernández, M. D., Kartal, D., Reichert, L., Burrows, J. P., Meyer Arnek, J., Lichtenstern, M., Stock, P., and Schlager, H.: Peroxy radical observations over West Africa during AMMA 2006: photochemical activity in the outflow of convective systems, Atmos. Chem. Phys., 9, 3681–3695, doi:10.5194/acp-9-3681-2009, 2009. 9658

Andrés-Hernández, M. D., Stone, D., Brookes, D. M., Commane, R., Reeves, C. E., Huntrieser, H., Heard, D. E., Monks, P. S., Burrows, J. P., Schlager, H., Kartal, D.,





AMTD
6, 9655–9688, 2013



Evans, M. J., Floquet, C. F. A., Ingham, T., Methven, J., and Parker, A. E.: Peroxy radical partitioning during the AMMA radical intercomparison exercise, Atmos. Chem. Phys., 10, 10621–10638, doi:10.5194/acp-10-10621-2010, 2010. 9658

Andrés-Hernández, M. D., Kartal, D., Crowley, J. N., Sinha, V., Regelin, E., Martínez-Harder, M., Nenakhov, V., Williams, J., Harder, H., Bozem, H., Song, W., Thieser, J., Tang, M. J., Hosaynali Beigi, Z., and Burrows, J. P.: Diel peroxy radicals in a semi-industrial coastal area: nighttime formation of free radicals, Atmos. Chem. Phys., 13, 5731–5749, doi:10.5194/acp-13-5731-2013, 2013. 9658

Bell, C. L., van Helden, J. P. H., Blaikie, T. P. J., Hancock, G., van Leeuwen, N. J., Peverall, R., and Ritchie, G. A. D.: Noise-immune cavity-enhanced optical heterodyne detection of $HO_2$ in the near-infrared range, J. Phys. Chem. A, 116, 5090–5099, 2012. 9657

Berden, G. and Engeln, R.: Cavity Ring-Down Spectroscopy: Techniques and Applications, John Wiley & Sons, Ltd, doi:10.1002/9781444308259.fmatter, 2010. 9660

Burkert, J., Andrés Hernández, M. D., Stöbener, D., Burrows, J. P., Weissenmayer, M., and Kraus, A.: Peroxy radical and related trace gas measurement in the marine boundary layer above the Atlantic Ocean, J. Geophys. Res., 106, 5457–5477, 2001a. 9657

Burkert, J., Behmann, T., Andrés Hernández, M. D., Weissenmayer, M., Perner, D., and Burrows, J. P.: Measurements of peroxy radicals in a forested area in Portugal, Chemosphere, 3, 3327–3338, 2001b. 9658

Burkert, J., Andrés Hernández, M. D., Reichert, L., Meyer-Arnek, J., Doddridge, B., Dickerson, R. R., Mühle, J., Zahn, A., Carsey, T., and Burrows, J. P.: Trace gas and radical behaviour in the marine boundary layer during INDOEX 1999, J. Geophys. Res., 108, INX2 35–1 to 35–18, doi:10.1029/2002JD002790, 2003. 9658

Busch, K. W. and Busch, M. A.: Cavity-Ringdown Spectroscopy, American Chemical Society, doi:10.1021/bk-1999-0720, 1999. 9660

Cantrell, C. A. and Stedman, D. H.: A possible technique for the measurement of atmospheric peroxy radicals, Geophys. Res. Lett., 9, 846–849, 1982. 9657

Cantrell, C. A., Stedman, D. H., and Wendel, G. J.: Measurement of atmospheric peroxy radicals by the chemical amplification, Anal. Chem., 56, 1496–1502, 1984. 9657

Cantrell, C. A., Zimmer, A., and Tyndall, G. S.: Absorption cross sections for water vapor from 183 to 193 nm, Geophys. Res. Lett., 24, 2195–2198, 1997. 9667





AMTD
6, 9655–9688, 2013



Chrobry, A.: Development and laboratory characterization of a sampling system for airborne measurements of peroxy radicals using chemical amplification, Ph. D. dissertation, University of Bremen, Bremen, 2013. 9661, 9663, 9669

Courtillot, I., Morville, J., Mottoros, V., and Romanini, D.: Sub-ppb $NO_2$ detection by optical feedback cavity-enhanced absorption spectroscopy with a blue diode laser, Appl. Phys. B, 85, 407–412, 2006. 9663

Djehiche, M., Tomas, A., Fittschen, C., and Coddeville, P.: First cavity ring-down spectroscopy $HO_2$ measurements in a large photoreactor, Z. Phys. Chem., 225, 983–992, doi:10.1524/zpch.2011.0143, 2011. 9657

Fuchs, H., Brauers, T., Häseler, R., Holland, F., Mihelcic, D., Müsgen, P., Rohrer, F., Wegener, R., and Hofzumahaus, A.: Intercomparison of peroxy radical measurements obtained at atmospheric conditions by laser-induced fluorescence and electron spin resonance spectroscopy, Atmos. Meas. Tech., 2, 55–64, doi:10.5194/amt-2-55-2009, 2009. 9657

Hargrove, J., Wang, L., Muyskens, K., Muyskens, M., Medina, D., Zaide, S., Zhang, J.: Cavity ring-down spectroscopy of ambient $NO_2$ with quantification and elimination of interferences, Env. Sci. Tech., 40, 7868–7873, 2006. 9658

Hastie, D. R., Weissenmayer, M., Burrows, J. P., and Harris, G. W.: Calibrated chemical amplifier for atmospheric $RO_x$ measurements, Anal. Chem., 63, 2048–2057, 1991. 9657

Heard, D.: Analytical Techniques for Atmospheric Measurement, Blackwell Publishing Ltd, 528 pp., 2006. 9657

Hofzumahaus, A., Brauers, T., Aschmutat, U., Brandenburger, U., Dorn, H. P., Hausmann, M., Heßling, M., Holland, F., Plass-Dülmer, C., Sedlacek, M., Weber, M., and Ehhalt, D. H.: Reply, Geophys. Res. Lett., 24, 3039–3040, 1997. 9667

Hofzumahaus, A., Rohrer, F., Lu, K., Bohn, B., Brauers, T., Chang, C.-C., Fuchs, H., Holland, F., Kita, K., Kondo, Y., Li, X., Lou, S., Shao, M., Zeng, L., Wahner, A., and Zhang, Y.: Amplified trace gas removal in the troposphere, Science, 324, 1702–1704, doi:10.1126/science.1164566, 2009. 9656, 9657

Horstjann, M., Nenakhov, V., and Burrows, J. P.: Frequency stabilization of blue extended cavity diode lasers by external cavity optical feedback, Appl. Phys. B, 106, 261–266, 2012. 9664, 9680

Kartal, D.: Characterization and optimization of a dual channel PERCA for the investigation of the chemistry of peroxy radicals in the upper troposphere, Ph. D. dissertation, University of Bremen, Bremen, 2009. 9667





AMTD
6, 9655–9688, 2013



Kartal, D., Andrés Hernández, M. D., Reichert, L., Schlager, H., and Burrows, J. P.: Technical Note: Characterisation of a DUALER instrument for the airborne measurement of peroxy radicals during AMMA 2006, Atmos. Chem. Phys., 10, 3047–3062, doi:10.5194/acp-10-3047-2010, 2010. 9658, 9661

Lelieveld, J., Butler, T. M., Crowley, J. N., Dillon, T. J., Fischer, H., Ganzeveld, L., Harder, H., Lawrence, M. G., Martinez, M., Taraborrelli, D., and Williams, J.: Atmospheric oxidation capacity sustained by a tropical forest, Nature, 452, 737–740, 2008. 9656

Liu, Y., Morales-Cueto, R., Hargrove, J., Medina, D., and Zhang, J.: Measurements of peroxy radicals using chemical amplification-cavity ringdown spectroscopy, Environ. Sci. Technol., 43, 7791–7796, 2009. 9658, 9670

Mihelcic, D., Müsgen, P., and Ehhalt, D. H.: An improved method of measuring tropospheric $NO_2$ and $RO_2$ by matrix isolation and electron spin resonance, J. Atmos. Chem., 3, 341–361, 1985. 9657

Monks, P.: Gas-phase radical chemistry in the troposphere, Chem. Soc. Rev., 34, 376–395, 2005. 9656

Morville, J., Kassi, S., Chenevier, M., and Romanini, D.: Fast, low-noise, mode-by-mode, cavity-enhanced absorption spectroscopy by diode-laser self-locking, Appl. Phys. B, 80, 1027–1038, 2005. 9663

Nizkorodov, S. A., Sander, S. P., and Brown, L. R.: Temperature dependence of high-resolution air-broadened absorption cross sections of $NO_2$ (415–525 nm), J. Phys. Chem. A, 108, 4864–4872, 2004. 9660

O'Keefe, A. and Deacon, D. A. G.: Cavity ring-down optical spectrometer for absorption measurements using pulsed laser sources, Rev. Sci. Instrum., 59, 2544–2551, 1988. 9660

Reichert, L., Andrés Hernández, M. D., Stöbener, D., Burkert, J., and Burrows, J. P.: Investigation of the effect of water complexes in the determination of peroxy radical ambient concentrations: implications for the atmosphere, J. Geophys. Res., 108, 4017, doi:10.1029/2002JD002152, 2003. 9662, 9667

Schultz, M., Heitlinger, M., Mihelcic, D., and Volz-Thomas, A.: Calibration source for peroxy radicals with built-in actinometry using $H_2O$ and $O_2$ photolysis at 185 nm, J. Geophys. Res. 100, 18811–18816, 1995. 9667

Stöbener, D.: Weiterentwicklung einer Peroxyradikalquelle für die Kalibration von $RO_2$-Messungen in Außenluft, Diploma thesis, University of Bremen, Bremen, 1999. 9667

Thrush, B. A.: The chemistry of the stratosphere, Rep. Prog. Phys., 51, 1341–1371, 1988. 9656





AMTD
6, 9655–9688, 2013



Vandaele, A. C., Hermans, C., Fally, S., Carleer, M., Colin, R., Mérienne, M.-F., Jenouvrier, A., and Coquart, B.: High-resolution Fourier transform measurement of the $NO_2$ visible and near-infrared absorption cross-section: temperature and pressure effects, J. Geophys. Res., 107, 4348, doi:10.1029/2001JD000971, 2002. 9660

Wendisch, M. and Brenguier, J.-L.: In situ trace gas measurements, in: Airborne Measurements for Environmental Research: Methods and Instruments, Wiley-VCH, Berlin, 611 pp., 2013. 9658

Whalley, L. K., Edwards, P. M., Furneaux, K. L., Goddard, A., Ingham, T., Evans, M. J., Stone, D., Hopkins, J. R., Jones, C. E., Karunaharan, A., Lee, J. D., Lewis, A. C., Monks, P. S., Moller, S. J., and Heard, D. E.: Quantifying the magnitude of a missing hydroxyl radical source in a tropical rainforest, Atmos. Chem. Phys., 11, 7223–7233, doi:10.5194/acp-11-7223-2011, 2011. 9656





AMTD
6, 9655–9688, 2013



**Table 1.** Abbreviations used in this paper.

| abbreviation | meaning |
|---|---|
| CL | **C**hain **L**ength |
| CRDS | **C**avity **R**ing-**D**own **S**pectroscopy |
| ECDL | **E**xtended **C**avity **D**iode **L**aser |
| HALO | **H**igh **A**ltitude and **LO**ng range research aircraft |
| OF-CEAS | **O**ptical **F**eedback **C**avity **E**nhanced **A**bsorption **S**pectroscopy |
| OMO | **O**xidation **M**echanisms, **O**bservations in the extra-tropical free troposphere |
| PeRCA | **Pe**roxy **R**adical **C**hemical **A**mplification |
| PeRCEAS | **Pe**roxy **R**adical **C**avity**E**nhanced **A**bsorption **S**pectroscopy |
| PMT | **P**hoto**M**ultiplier **T**ube |
| PFA | **P**er**F**luor**A**lkoxy |
| PAN | **P**eroxy**A**cetyl **N**itrate |
| PTFE | **P**oly**T**etra**F**luor**E**thylene |
| pptv, ppbv, ppmv | **p**arts **p**er **t**rillion/**b**illion/**m**illion of volume |
| roc | **r**adius **o**f **c**urvature |
| sLpm | **s**tandard ($p_{st}$ = 1013 mbar, $T_{st}$ = 273.15 K) **L**itres **p**er **m**inute |





AMTD
6, 9655–9688, 2013



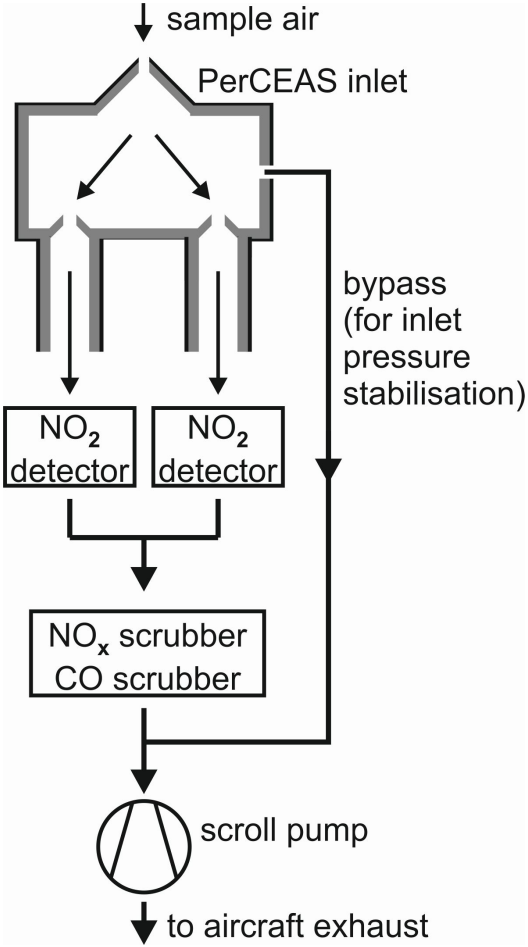


**Fig. 1.** Sample air flow in the PeRCEAS instrument.





AMTD
6, 9655–9688, 2013

Airborne peroxy radical detection by cavity enhanced $NO_2$ spectroscopy

M. Horstjann et al.



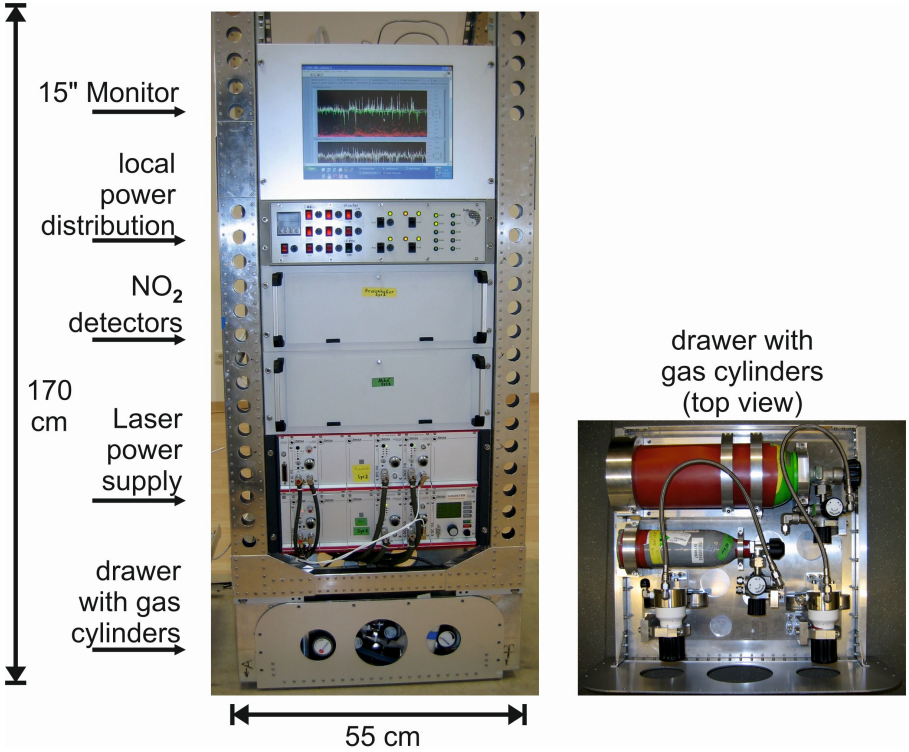


**Fig. 2.** PeRCEAS rack front side. Rack components which are not visible: PXI computer, temperature –, pressure – and flow controllers, and HALO power supply unit.





AMTD
6, 9655–9688, 2013



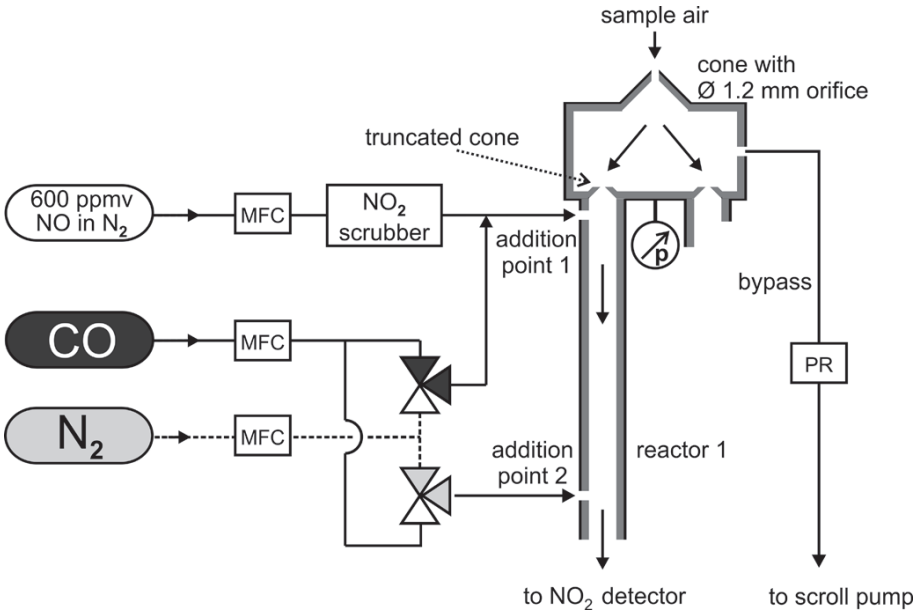


**Fig. 3.** Schematic diagram of the PeRCEAS inlet with one reactor shown in amplification mode (the other reactor is whitened out). MFC – mass flow controller, PR – pressure regulator.





AMTD
6, 9655–9688, 2013



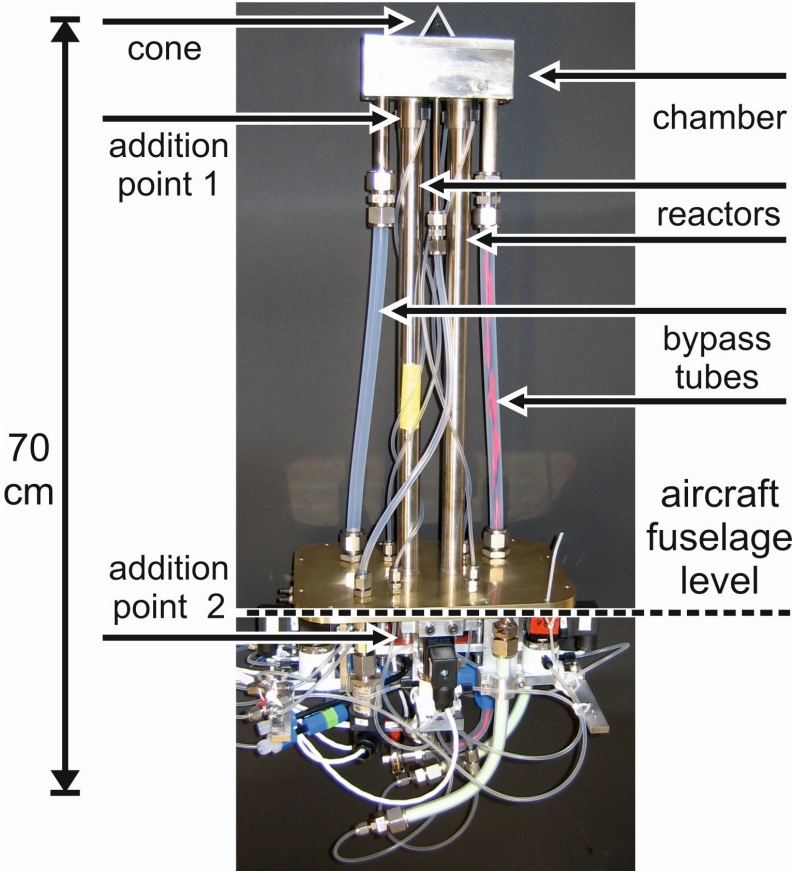


**Fig. 4.** Side view of the PeRCEAS inlet. Not shown: outer aircraft protection pylon and inner aircraft protection casing.





AMTD
6, 9655–9688, 2013



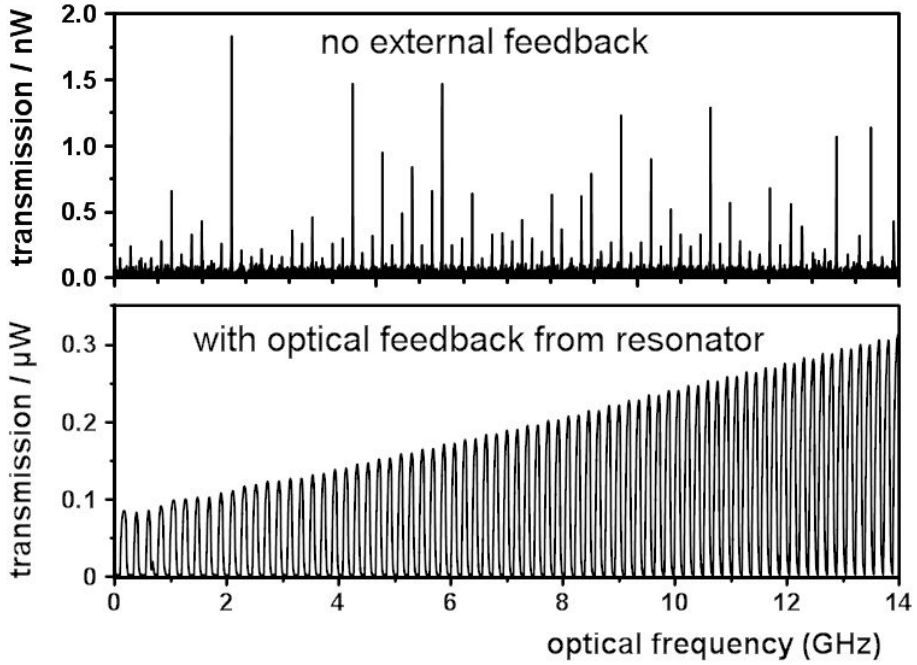


**Fig. 5.** Resonator transmission vs. relative laser frequency (at a wavelength of 408.9 nm) during a piezo scan of the laser grating (Horstjann et al., 2012). (Top) Freely running extended cavity diode laser. (Bottom) With optical feedback from the high-finesse V-resonator. The signal slope is due to higher laser power at the end of the wavelength scan.





AMTD
6, 9655–9688, 2013



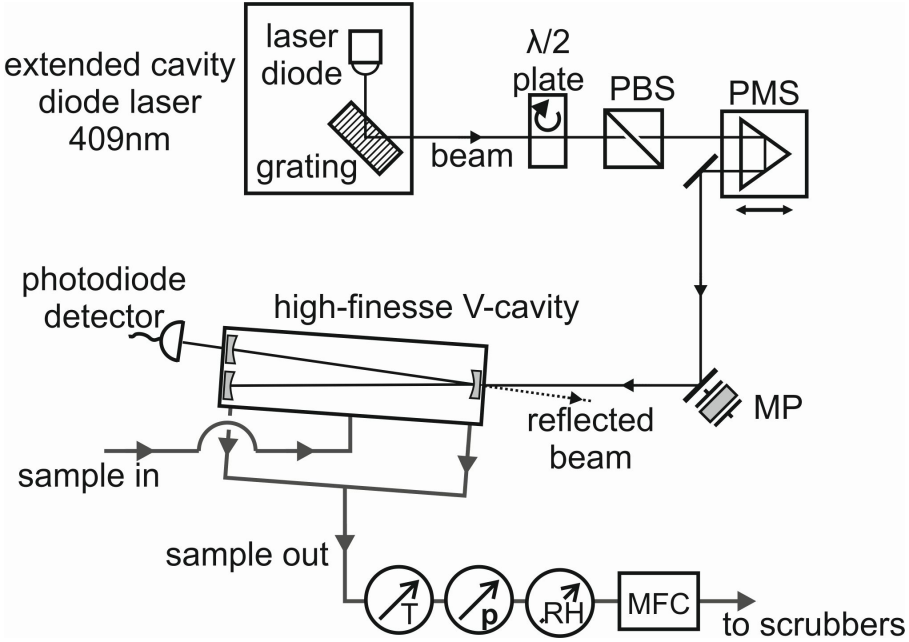


**Fig. 6.** Schematic diagram of a PeRCEAS $NO_2$ detector. PBS – polarizing beamsplitter, PMS – prism with micrometer screw, MP – mirror with piezo, MFC – mass flow controller. The sensors shown measure the temperature ($T$), pressure ($p$) and relative humidity (RH) of the sample gas.





AMTD
6, 9655–9688, 2013



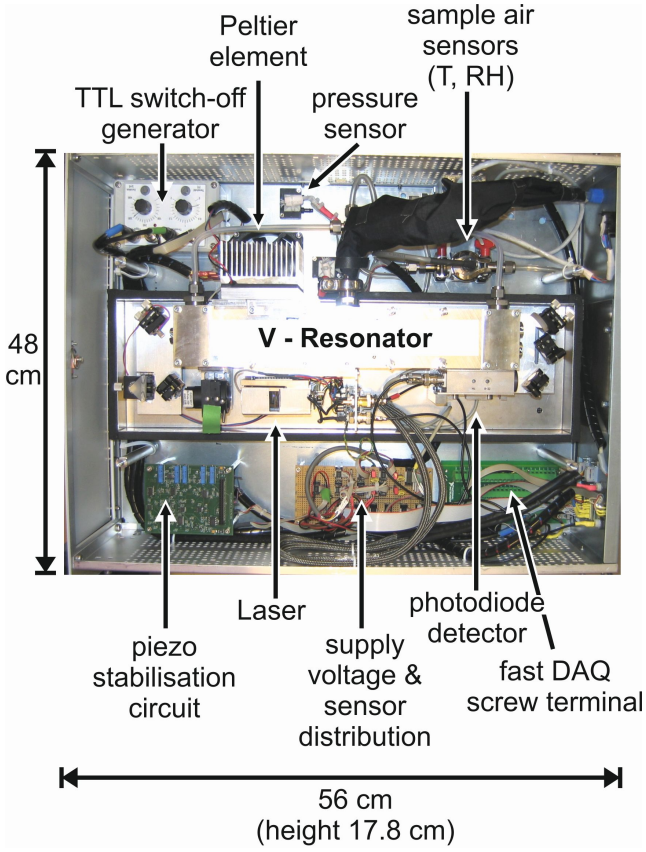


**Fig. 7.** Top view of the PeRCEAS $NO_2$ detector. The detector fits inside a 4 height units 19″ case whose front (here: left side) can be opened. All electrical and gas connections are on its back side (here: right side).





AMTD
6, 9655–9688, 2013



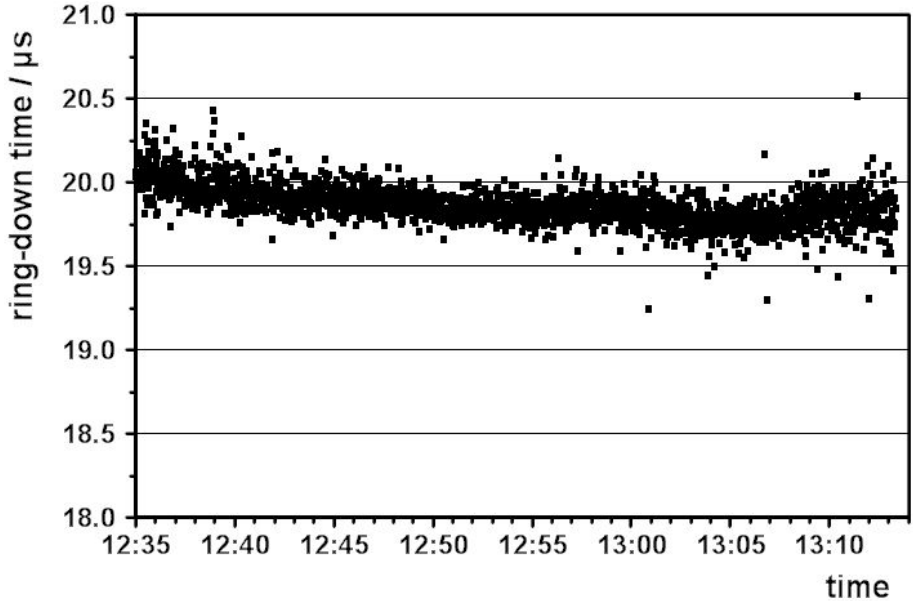


**Fig. 8.** Ring-down measurement of a constant background signal provided by a synthetic air flow of 1 sLpm through the resonator.





AMTD
6, 9655–9688, 2013



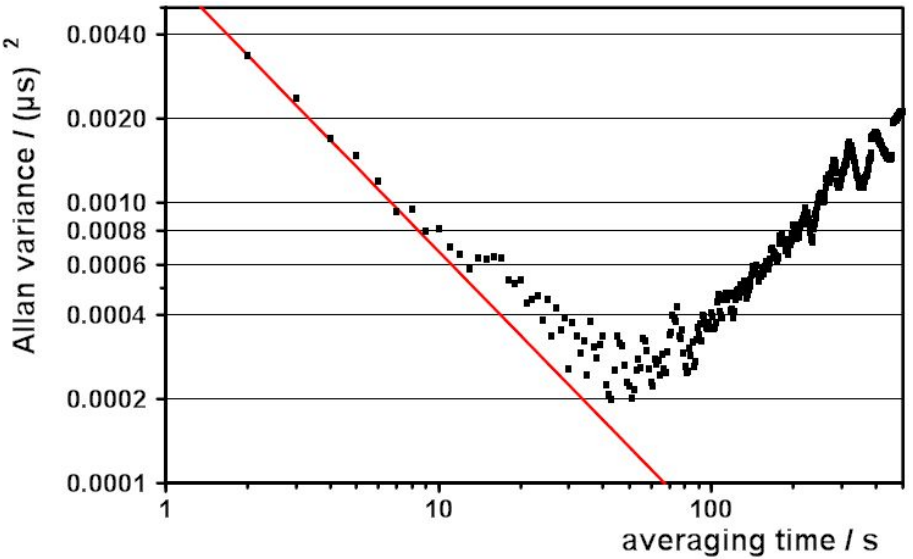


**Fig. 9.** Allan variance of the synthetic air measurement as depicted in Fig. 8.The red line indicates a slope of −1.0 which is expected for white noise only.





AMTD
6, 9655–9688, 2013



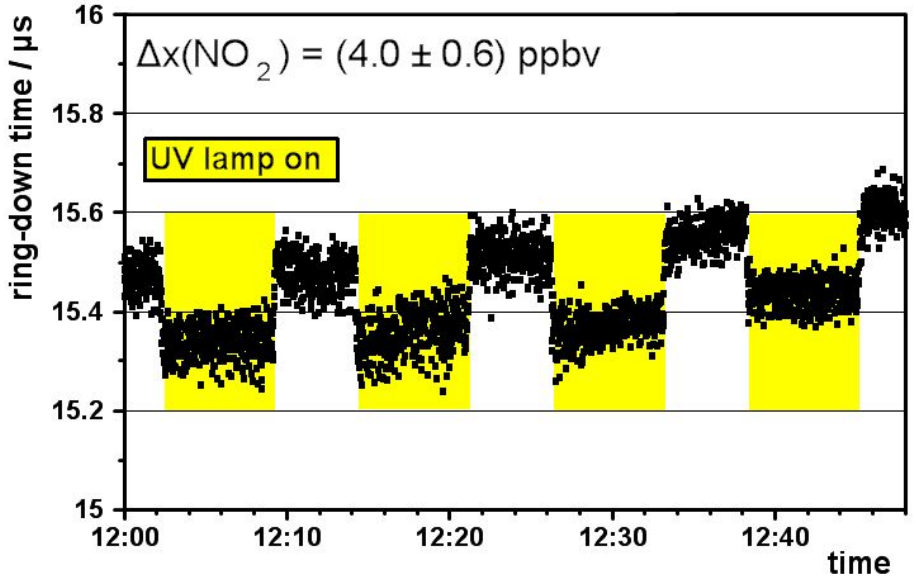


**Fig. 10.** Measurement of the maximum ozone concentration generated by the radical source.





AMTD
6, 9655–9688, 2013



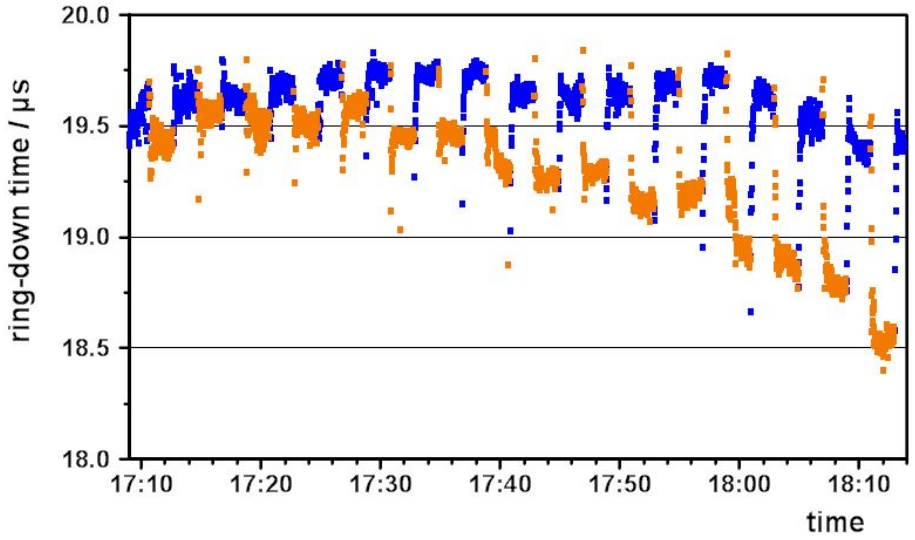


**Fig. 11.** $HO_2$ calibration measurement at an inlet pressure of 300 mbar. Blue – background, orange – amplification mode as determined by the reactor configuration.





AMTD
6, 9655–9688, 2013



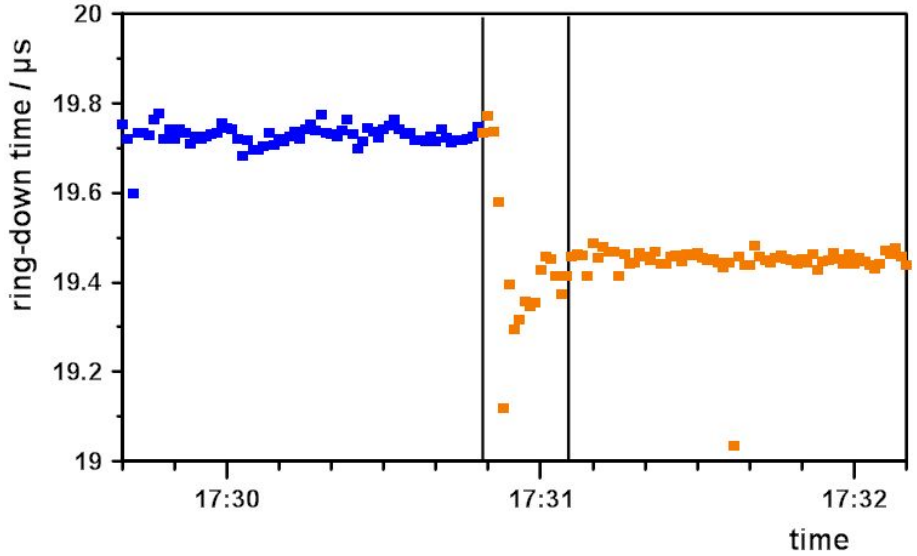


**Fig. 12.** Switching between background (blue) and amplification mode (orange); the two solid lines indicate a time difference of 16 s required for the gas flow stabilization.





AMTD
6, 9655–9688, 2013



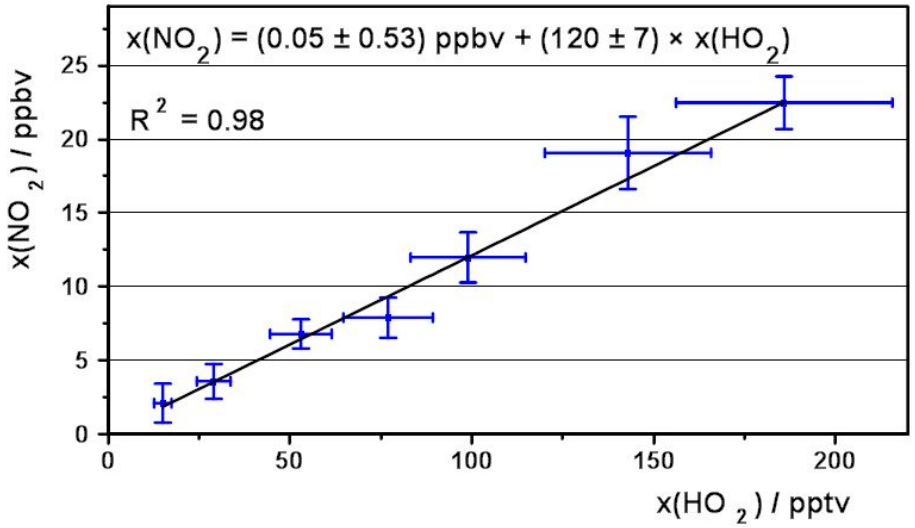


**Fig. 13.** Chain length determination corresponding to the calibration measurement shown in Fig. 11. Shown are the $NO_2$ – vs. $HO_2$ mixing ratios. The slope of the linear fit is the chain length.





AMTD
6, 9655–9688, 2013